

Hadrophilic dark sectors at the Forward Physics Facility

Brian Batell,^{1,*} Jonathan L. Feng^{2,†} Max Fieg,^{2,‡} Ahmed Ismail,^{3,§} Felix Kling^{4,5,||}
Roshan Mammen Abraham^{6,¶} and Sebastian Trojanowski^{6,7,**}

¹*Pittsburgh Particle Physics, Astrophysics, and Cosmology Center, Department of Physics and Astronomy,
University of Pittsburgh, Pittsburgh, Pennsylvania 15217, USA*

²*Department of Physics and Astronomy, University of California, Irvine, California 92697-4575, USA*

³*Department of Physics, Oklahoma State University, Stillwater, Oklahoma 74078, USA*

⁴*Theory Group, SLAC National Accelerator Laboratory, Menlo Park, California 94025, USA*

⁵*Deutsches Elektronen-Synchrotron DESY, Notkestrasse 85, 22607 Hamburg, Germany*

⁶*Astrocent, Nicolaus Copernicus Astronomical Center Polish Academy of Sciences,
ul. Rektorska 4, 00-614 Warsaw, Poland*

⁷*National Centre for Nuclear Research, ul. Pasteura 7, 02-093 Warsaw, Poland*



(Received 1 December 2021; accepted 7 March 2022; published 5 April 2022)

Models with light dark sector and dark matter particles motivate qualitatively new collider searches. Here we carry out a comprehensive study of hadrophilic models with $U(1)_B$ and $U(1)_{B-3L_\tau}$ gauge bosons coupled to light dark matter. The new mediator particles in these models couple to quarks, but have suppressed couplings to leptons, providing a useful foil to the well-studied dark photon models. We consider current bounds from accelerator and collider searches, rare anomaly-induced decays, neutrino nonstandard interactions, and dark matter direct detection. Despite the many existing constraints, these models predict a range of new signatures that can be seen in current and near future experiments, including dark gauge boson decays to the hadronic final states $\pi^+\pi^-\pi^0$, $\pi^0\gamma$, K^+K^- , and $K_S K_L$ in FASER at LHC Run 3, enhancements of ν_τ scattering rates in far-forward neutrino detectors, and thermal dark matter scattering in FLArE in the HL-LHC era. These models therefore motivate an array of different experiments in the far-forward region at the LHC, as could be accommodated in the proposed Forward Physics Facility.

DOI: [10.1103/PhysRevD.105.075001](https://doi.org/10.1103/PhysRevD.105.075001)

I. INTRODUCTION

Searches for new particles and dark matter (DM) are primary physics drivers at the Large Hadron Collider (LHC). Traditional searches for the classic missing p_T signature at the LHC main detectors have sensitively searched for particles with weak-scale masses and $\mathcal{O}(1)$ couplings to Standard Model (SM) particles but are less effective for light and weakly coupled new particles, including long-lived particles (LLPs) and DM. Recently it has been appreciated that new experiments in the far-forward region at the LHC can provide a powerful probe of

new light particles. These experiments exploit the large forward flux of pions and other SM particles, which, if they decay to new light particles, can create a large forward flux of LLPs and DM. Light new physics species can also be produced in the far-forward region of the LHC in other types of interactions, including proton-proton bremsstrahlung and the Drell-Yan process. The recent detection of TeV neutrino candidates in the forward region [1] also opens a new window on neutrinos at colliders, which may be used to probe both SM and beyond the SM (BSM) phenomena [2–4].

In evaluating any proposal for new physics at the MeV to GeV mass scale, one must carefully consider all of the existing constraints from particle and nuclear experiments carried out over the last 60 years. To do this requires a model framework. The dark photon model has been discussed at length in the literature. It is theoretically attractive and contains within it phenomenologically viable benchmark scenarios of light thermal DM. Of particular relevance for this study, previous studies in the dark photon framework have established the potential for forward experiments to detect both LLPs [5,6] and light thermal DM [7,8]. At the same time, the experimental signatures of a given dark sector model are, to a large extent, determined

*batell@pitt.edu

†jlf@uci.edu

‡mfieg@uci.edu

§aismail3@okstate.edu

||felix.kling@desy.de

¶rmammen@okstate.edu

**strojanowski@camk.edu.pl

Published by the American Physical Society under the terms of the [Creative Commons Attribution 4.0 International license](https://creativecommons.org/licenses/by/4.0/). Further distribution of this work must maintain attribution to the author(s) and the published article's title, journal citation, and DOI. Funded by SCOAP³.

by the interactions of the mediator with the SM. To more fully evaluate the physics potential of proposed experiments, then, a variety of phenomenologically distinct mediators must be examined. Since the LHC is a pp collider, it is natural to consider mediators with hadrophilic couplings, i.e., sizable couplings to quarks, but suppressed couplings to leptons. Although such models are challenging to test at electron facilities (e.g., Belle-II [9], NA64 [10], LDMX [11], and SENSEI [12]), one might suspect that they can be sensitively probed at proton facilities, such as the LHC.

In this work we study the prospects for probing two dark sector models with hadrophilic vector boson mediators. The first model is based on a gauged $U(1)_B$ baryon number symmetry (see, e.g., Refs. [13–17]). This model is perhaps the first example of a hadrophilic model one might consider, since it has sizable couplings to quarks and (loop-)suppressed couplings to all leptons. The model suffers from gauge anomalies, however, which potentially lead to stringent constraints from rare flavor changing neutral currents (FCNC) and Z boson decays [18,19]. We will evaluate the prospects for discovering new physics in this model, carefully respecting all anomaly constraints, as well as those from other experimental searches. We note that anomaly-free extensions of the SM with a local $U(1)_B$ symmetry and DM have been constructed in Refs. [20–23], which focus on the case of new particle masses above the weak scale.

As a second example we consider a model with a $U(1)_{B-3L_\tau}$ vector boson mediator. [In the rest of this paper, we will use the modest abbreviation of $U(1)_{B-3\tau}$ for this symmetry.] With the addition of a right-handed neutrino, this symmetry is anomaly free and therefore evades the most stringent rare decay constraints present in the $U(1)_B$ model. This model is also hadrophilic, in the sense that couplings to electrons, muons, and their accompanying neutrinos are suppressed. However, the presence of τ and ν_τ couplings brings with it both additional constraints from neutrino nonstandard interactions (NSI), and also new opportunities for signals involving the third generation leptons. A goal of this study is to incorporate all these new constraints and see what discovery prospects remain.

We will consider both current and proposed far-forward experiments. In the last two years, the magnetic spectrometer and tracking detector FASER [24], and the two emulsion detectors FASER ν [25] and SND@LHC [26] have been approved. FASER has been fully constructed, and all three are expected to begin taking data when Run 3 starts in 2022. For the high luminosity LHC (HL-LHC) era, detectors under consideration include upgrades of these detectors (FASER2, FASER ν 2, and Advanced SND), as well as the Forward Liquid Argon Experiment (FLArE) [7].¹ A new facility, the

Forward Physics Facility (FPF) [4,29], has been proposed to accommodate these experiments.

Remarkably, we will find that all of these detectors have discovery prospects for the hadrophilic models we consider. The possible signals include DM deep inelastic scattering (DIS) and elastic scattering, enhanced predictions for neutrino neutral current (NC) scattering, an excess of tau neutrinos in the forward region, and the visible decay of the dark mediators into SM final states. Notably, the visible decays include final states, such as $\pi^+\pi^-\pi^0$, $\pi^0\gamma$, K^+K^- , and $K_S K_L$, that could conceivably appear in FASER at LHC Run 3; such states are inaccessible at FASER in dark photon models. The signals are diverse and require a similarly diverse set of experiments to find them, and when combined, the experiments probe parameter space even beyond the DM thermal targets. These models therefore add to the broad physics portfolio of the FPF, complementing other studies of long-lived particle searches, collider-produced TeV-energy neutrinos, new probes of QCD, and high-energy astroparticle physics [4].

The paper is organized as follows. In Sec. II we introduce the two hadrophilic dark sector models based on the $U(1)_B$ and $U(1)_{B-3\tau}$ gauge symmetries and discuss the production and decays of the vector boson mediator, the DM thermal relic abundance, and the existing constraints for each model. Next, we present our assumptions regarding the performance of FASER, FASER2, SND@LHC, FASER ν 2, and FLArE in Sec. III. In Sec. IV we outline our methodology for estimating the sensitivity of these far-forward detectors to the new physics signatures predicted in these hadrophilic models. Our main results are contained in Sec. V, and our conclusions and outlook are presented in Sec. VI.

II. MODELS OF HADROPHILIC PHYSICS

A. Models

With the motivation outlined in Sec. I, we begin in this section by describing the two representative hadrophilic dark sector models based on the anomalous $U(1)_B$ and anomaly-free $U(1)_{B-3\tau}$ gauge symmetries.² Since the new gauge group is Abelian, the new vector gauge boson generically mixes with the SM photon through a kinetic mixing term $F_{\mu\nu}V^{\mu\nu}$, where $F_{\mu\nu}$ and $V_{\mu\nu}$ are the field strengths of the SM photon and new gauge boson,

¹As a potential upgrade of milliQan [27], a fifth experiment, FORMOSA [28], has also been proposed to carry out dedicated searches for millicharged particles and similar signatures.

²The cancellation of gauge anomalies in the $U(1)_{B-3\tau}$ model requires the introduction of a right-handed neutrino with $B-3\tau$ charge of -3 . In this study we assume that the right handed neutrino is somewhat heavier than the vector boson mediator, which can be achieved by coupling it to the dark Higgs field that spontaneously breaks $U(1)_{B-3\tau}$. In principle the heavy neutrino mass could reside anywhere in the range below m_V/g_V . Depending on its mass and mixing with SM neutrinos there could be additional signatures beyond the core phenomenology outlined below. These are beyond the scope of our study, but see Ref. [30] for the sub-GeV case and far-forward searches.

respectively. In the physical mass basis, the Lagrangian of the vector boson mediator V_μ is

$$\mathcal{L} \supset -\frac{1}{4} V_{\mu\nu} V^{\mu\nu} + \frac{1}{2} m_V^2 V_\mu V^\mu + V_\mu (J_{\text{SM}}^\mu + J_\chi^\mu), \quad (1)$$

where m_V is the vector boson mass, J_{SM}^μ is a current composed of SM fields, and J_χ^μ is the current for the dark matter particle χ .

The SM current is

$$J_{\text{SM}}^\mu = g_V [J_B^\mu - 3x(\bar{\tau}\gamma^\mu\tau + \bar{\nu}_\tau\gamma^\mu P_L\nu_\tau)] + \epsilon e J_{\text{EM}}^\mu, \quad (2)$$

where $g_V \equiv \sqrt{4\pi\alpha_V}$ is the new U(1) gauge coupling, J_B^μ and J_{EM}^μ are the baryon number and electromagnetic currents, respectively, ϵ is the kinetic mixing parameter, and $x = 0$ (1) for the U(1)_B (U(1)_{B-3 τ}) model.

To specify J_χ^μ , we must choose the DM candidate χ . We will study both complex scalar DM and Majorana fermion DM in this work, with Lagrangians

$$\mathcal{L} \supset \begin{cases} |\partial_\mu\chi|^2 - m_\chi^2|\chi|^2, & \text{complex scalar} \\ \frac{1}{2}\bar{\chi}i\gamma^\mu\partial_\mu\chi - \frac{1}{2}m_\chi\bar{\chi}\chi, & \text{Majorana fermion} \end{cases}, \quad (3)$$

where m_χ is the DM mass. The associated currents, J_χ^μ in Eq. (1), are

$$J_\chi^\mu = g_V Q_\chi \begin{cases} i\chi^*\overleftrightarrow{\partial}^\mu\chi, & \text{complex scalar} \\ \frac{1}{2}\bar{\chi}\gamma^\mu\chi, & \text{Majorana fermion} \end{cases}, \quad (4)$$

where Q_χ is the charge of the DM under the new gauge symmetry. As we will discuss below, both complex scalar and Majorana fermion DM exhibit velocity-suppressed P -wave annihilation to SM final states, implying that bounds from precision measurements of the cosmic microwave background anisotropies [31,32] are easily satisfied in these models. Furthermore, Majorana DM features momentum-dependent scattering in the nonrelativistic regime, making it challenging to probe with DM direct detection experiments. This is not the case for complex scalar DM, and, as we will see, direct detection experiments place strong constraints on such DM for masses above the GeV scale. However, it is important to note that these constraints can also be evaded in a straightforward way by introducing a small mass splitting, which renders the scattering transition inelastic [33–35].

The full parameter space of these models is, then, specified by five parameters:

$$m_V, \quad g_V, \quad \epsilon, \quad m_\chi, \quad \text{and} \quad Q_\chi. \quad (5)$$

To reduce the parameter space, as is commonly done in the literature, we will assume a kinetic mixing parameter of typical one-loop size,

$$\epsilon = \frac{eg_V}{16\pi^2}. \quad (6)$$

This is the parametric size of the kinetic mixing generated by loops of SM particles charged under both electromagnetism and the new gauge symmetry. The kinetic mixing depends, in general, on the details of the UV physics and therefore cannot be determined unambiguously, but we neglect such effects here; see also Ref. [36] for further discussion of this issue. Throughout our study we will also adopt another common convention,

$$m_V = 3m_\chi, \quad (7)$$

so that DM annihilation proceeds to SM particles through a virtual s -channel vector boson mediator.

Given the assumptions of Eqs. (6) and (7), the resulting parameter space may be specified by the three parameters

$$m_V, \quad g_V, \quad \text{and} \quad Q_\chi. \quad (8)$$

We will present our results in the (m_V, g_V) plane with various choices for Q_χ . Since the new symmetries are Abelian, the charge Q_χ may be any real number. When presenting our results below, we will consider two choices for coupling hierarchies. As a first scenario, we will consider DM and SM particles to have comparable interaction strengths with the vector boson mediator, fixing

$$Q_\chi = \begin{cases} 1, & \text{U(1)}_B \text{ models} \\ 3, & \text{U(1)}_{B-3\tau} \text{ models} \end{cases}. \quad (9)$$

In the $B - 3\tau$ model, we have fixed the DM charge to be opposite that of the ν_τ , $Q_\chi = -Q_\tau$. As a second, qualitatively distinct, scenario, we consider the case in which the DM coupling to the vector boson mediator has a fixed value,

$$\alpha_\chi \equiv \frac{g_V^2 Q_\chi^2}{4\pi} = 0.01 \quad \text{or} \quad 0.5. \quad (10)$$

Given that we will be considering vector boson mediators with weak couplings to the SM, that is, values of $g_V \sim 10^{-8}$ – 10^{-2} , Eq. (10) implies very large DM charges Q_χ . This may appear unnatural, but there is nothing wrong in principle, since the expansion parameter α_χ remains perturbative. Ideas for achieving such large coupling hierarchies for two U(1) gauge symmetries have been presented in Ref. [37].

Finally, although we do not consider them in this work, viable models of hadrophilic scalar mediators can also be constructed; see, e.g., Refs. [38–40]. However, for the incident DM energies in the TeV range relevant for FPF experiments, scalar-mediated DM-nuclear scattering rates are typically suppressed by several orders of magnitude in

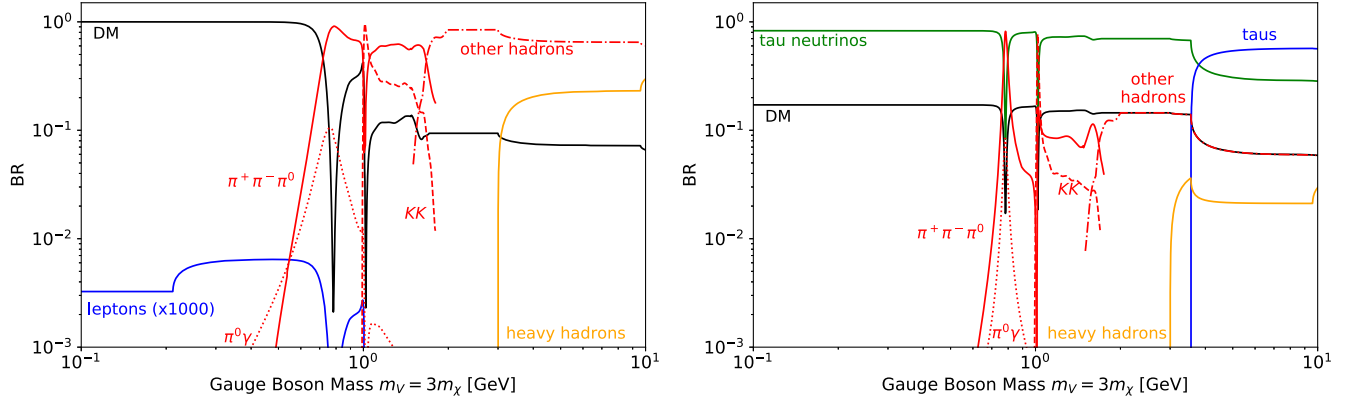


FIG. 1. Decay branching fractions of the B (left) and $B - 3\tau$ (right) gauge bosons for fixed $Q_\chi = 1$ and 3 , respectively. The “heavy hadrons” contour includes charm and bottom hadrons, and the red contours correspond to all other hadrons. Among them, we explicitly show the dominant branching fractions into $\pi^0\pi^+\pi^-$, $\pi^0\gamma$, and kaon pairs $KK = K^+K^- + K_S K_L$. Here we assume loop-induced couplings of the bosons to charged leptons of the first two generations of size $g_\ell = g_V(e/4\pi)^2$. The relevant contour for boson decays into e^+e^- or $\mu^+\mu^-$, shown in the left panel, has been multiplied by a factor of 1000 for visibility. The DM is taken to be a scalar, with the decay width given in Eq. (11).

comparison to vector boson-mediated scattering rates; see also Ref. [37] for a comparison of vector boson- and scalar-mediated DM scattering in the ultrarelativistic regime. For this reason, scalar-mediated DM scattering can be better probed by low- and medium-energy experiments [39]. On the other hand, experiments such as FASER and FASER2 can have powerful sensitivity to visible decays of the long-lived scalar mediator in these models, as has been demonstrated in Ref. [41].

B. Production and decay of the vector boson mediator

In our simulations, we model the production of light dark vector bosons in the far-forward region of the LHC by employing the FORESEE package [41]. We thereby include dark vector boson production by light meson decays, proton bremsstrahlung,³ and the Drell-Yan process. We observe that typically the production of dark vector bosons in light meson decays dominates if kinematically allowed. For the dark vector bosons heavier than the η meson, the most important production mode is due to bremsstrahlung, while the Drell-Yan process starts to dominate for $m_V > 1.5$ GeV.

We then consider various decay final states of the dark vector bosons. In particular, the partial decay width for $V \rightarrow \chi\chi^*$ is

$$\Gamma_{\chi\chi^*} = \kappa \frac{\alpha_\chi m_V}{12} \left(1 - \frac{4m_\chi^2}{m_V^2}\right)^{3/2}, \quad (11)$$

where $\kappa = 1$ and 2 for complex scalar and Majorana DM, respectively. The partial decay width into hadrons and other SM particles is taken from the DARKCAST package [45], which used data-driven methods to estimate the hadronic width. An alternative description has also recently been implemented in HERWIG 7, see Ref. [46].

In Fig. 1, we present the corresponding decay branching fractions for both of the models assuming the Q_χ charge as in Eq. (9). In the case of the $U(1)_B$ model, LLP decays into lepton pairs are always subdominant, since they appear only at the loop level through the vector boson mixing with the photon. In contrast, the invisible branching fraction of $V \rightarrow \chi\chi^*$ is close to unity for light vector boson masses up to the ω -resonance region, $m_V \approx m_\omega \simeq 782$ MeV. This leads to an intense flux of DM particles, which can be detected via DM scatterings, as we will discuss in Secs. IV A and IV B. For heavier dark vector bosons, decays into light hadrons start to play an important role and can lead to additional signatures in the detectors, as we will see in Sec. IV E.

For the $B - 3\tau$ model with the dark charge set to $Q_\chi = 3$, we obtain $\text{BR}(V \rightarrow \chi\chi^*) \sim (10 - 20)\%$ up to the tau threshold, above which $V \rightarrow \tau^+\tau^-$ decays become kinematically allowed. The remaining decay rate for lighter dark vector bosons is dominantly into tau neutrinos, $V \rightarrow \nu_\tau \bar{\nu}_\tau$. As will be discussed in Sec. IV D, this can contribute to the total ν_τ flux measured at the FPF. The decays into hadrons also become important for certain values of m_V , especially around the ω - and ϕ -resonance regions.

C. Thermal relic abundance

Thermal targets, that is, the regions of parameter space where DM annihilates in the early Universe through

³The modeling of dark vector boson production via proton bremsstrahlung in FORESEE is based on the Fermi-Weizsacker-Williams approximation presented in Refs. [42,43]. Recently, Ref. [44] studied this process using an alternative model of nucleon interactions based on Pomeron exchange, finding production rates that are smaller by a factor of a few. These estimates provide a sense of the theoretical uncertainty inherent in this process.

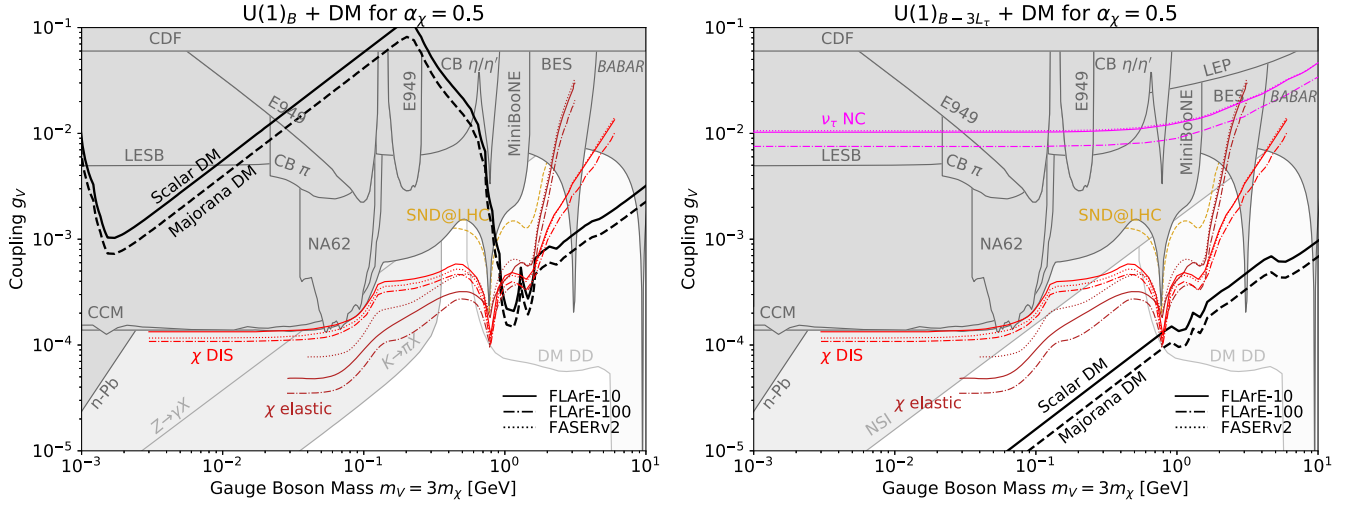


FIG. 2. The (m_V, g_V) parameter space of hadrophilic DM models with $U(1)_B$ (left) and $U(1)_{B-3L_\tau}$ (right) gauge boson mediators coupling to complex scalar DM, for dark matter coupling $\alpha_\chi = 0.01$ (top) and 0.5 (bottom), and $m_V = 3m_\chi$. The black contours are the thermal relic targets for complex scalar and Majorana DM; DM is thermally overproduced below these contours. The light (dark) red lines correspond to 90% confidence limits (C.L.) exclusion bounds from DM DIS (elastic) scatterings off nuclei for FLArE-10, FLArE-100, and FASERV2, as indicated. The dotted brown contours are the sensitivity contours for SND@LHC [49]. In the right panels, the light purple contours are the projected sensitivity contours from probing the V -induced BSM NC interactions of tau neutrinos. In both panels, the dark gray shaded regions are excluded by current bounds. The light gray shaded regions in the left (right) panels correspond to the anomaly-induced K and Z decays (NSI bounds). The very light gray shaded regions are constraints from DM DD; these do not apply to Majorana and inelastic scalar DM (see Sec. II D).

thermal freeze-out to the correct relic density, provide an important standard by which to judge the sensitivity of collider searches. These have been determined in the $U(1)_B$ model with fixed $\alpha_\chi = 0.5$ in Ref. [37]. Here we determine, for the first time, the thermal targets for the $U(1)_B$ model with fixed Q_χ and for the $U(1)_{B-3\tau}$ model described above.

The dark matter annihilation cross section can be written in the standard resonance form,

$$\sigma_{\text{ann}}(s) = \kappa \frac{16\pi (2s_V + 1)}{s\beta_\chi^2 (2s_\chi + 1)^2} \frac{s\Gamma_{\chi\chi^*}(s)\Gamma_{\text{SM}}(s)}{(s - m_V^2)^2 + m_V^2\Gamma_V^2}, \quad (12)$$

where $\beta_\chi(s) = (1 - 4m_\chi^2/s)^{1/2}$, $s_V = 1$, $s_\chi = 0$, and $\Gamma_{\chi\chi^*}(s)$ and $\Gamma_{\text{SM}}(s)$ are the partial decay widths for V decaying into dark matter and SM particles, respectively, with the replacement $m_V \rightarrow \sqrt{s}$.

The thermally averaged cross section is, then, [47]

$$\langle\sigma_{\text{ann}}v\rangle = \frac{\kappa \int_{4m_\chi^2}^{\infty} (s - 4m_\chi^2) \sigma_{\text{ann}}(s) K_1(\sqrt{s}/T) ds}{2 \cdot 8m_\chi^4 K_2^2(m_\chi/T)}, \quad (13)$$

where v is the relative velocity of the annihilating dark matter particles, and K_i is the modified Bessel function of order i . To determine the thermal target regions of parameter space, we require

$$\langle\sigma_{\text{ann}}v\rangle = 4 \times 10^{-26} \text{ cm}^3 \text{ s}^{-1}, \quad (14)$$

which reproduces the observed DM relic abundance for the masses we consider [48].

The thermal targets are presented below in Figs. 2 and 3. Their shapes can be understood as follows. In the $U(1)_{B-3\tau}$ models, annihilation to tau neutrinos is allowed throughout the m_V range. The thermally averaged cross section has the parametric dependence

$$\langle\sigma_{\text{ann}}v\rangle \sim \frac{\kappa g_V^4 Q_\chi^2}{m_V^2} \sim \frac{\kappa g_V^2 \alpha_\chi}{m_V^2}, \quad (15)$$

and so in the $(\log m_V, \log g_V)$ plane, the thermal targets have slope 1 for the models with fixed α_χ shown in Fig. 2, and slope 1/2 for the models with fixed Q_χ shown in Fig. 3. The discrepancy between the complex scalar and Majorana fermion cases results from the fact that in the complex scalar case, there are both DM and anti-DM particles, whereas in the Majorana case, DM is its own antiparticle, which impacts the annihilation rate through the parameter κ 's appearance in Eqs. (12) and (13).

For the $U(1)_B$ models, the thermal target slopes are similar to those for the $U(1)_{B-3\tau}$ models for $m_V \gtrsim 1$ GeV. The required couplings g_V are greater because the annihilation to tau neutrinos is absent. As m_V drops below 1 GeV, the cross section to hadrons decreases rapidly, and without a large leptonic annihilation channel, the required g_V increases rapidly to maintain a fixed $\langle\sigma_{\text{ann}}v\rangle$. This continues until m_V drops below m_{π^*} , at which point all hadronic channels shut off, and only the loop-suppressed annihilation to light

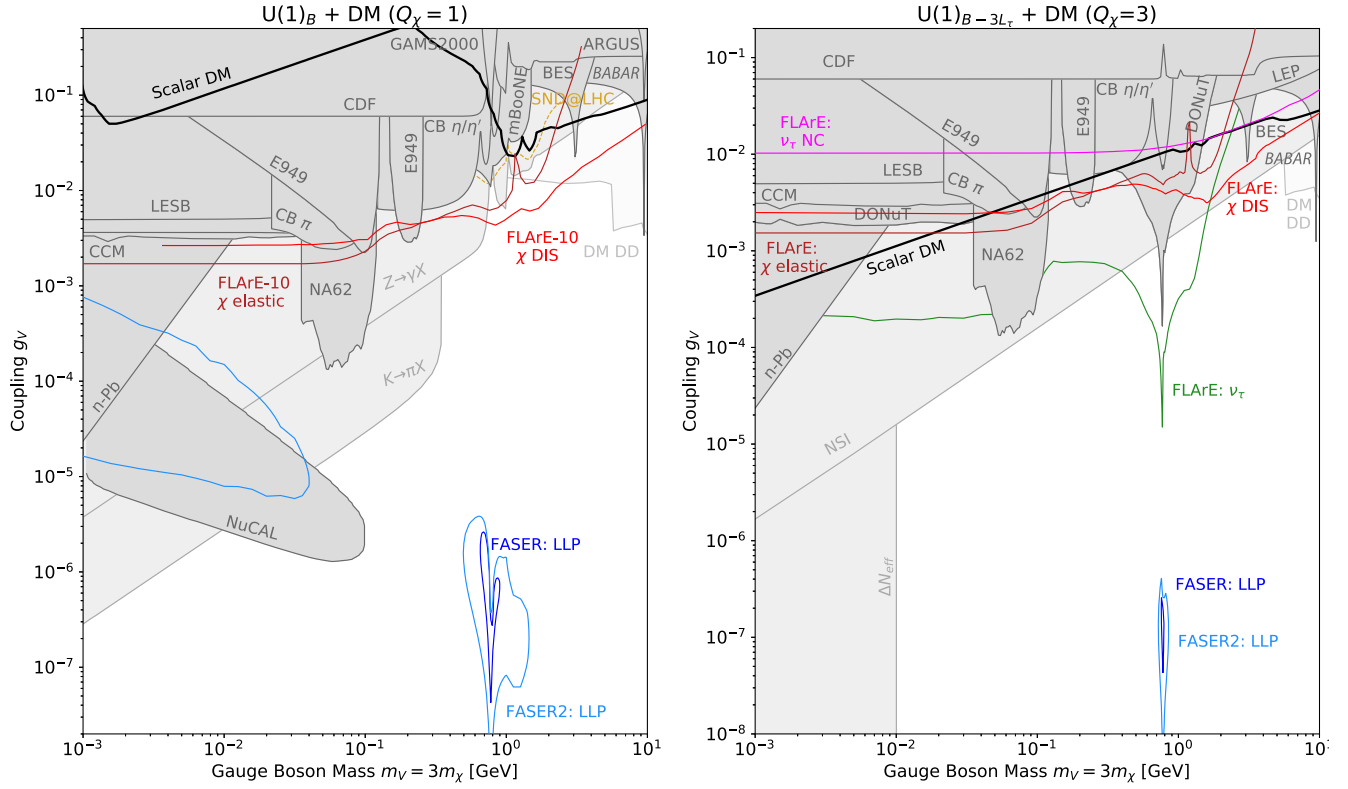


FIG. 3. Same as Fig. 2, but for only the FLArE-10 detector, complex scalar DM, and fixed charges $Q_\chi = 1$ (left) and $Q_\chi = -Q_\tau = 3$ (right), resulting in a floating α_χ . Additional expected exclusion bounds from probing displaced V decays to SM final states in FASER (FASER2) are shown with dark (light) blue lines. In the right panel, the green contour is the sensitivity contour from probing excess CC scatterings of ν_τ .

leptons is allowed. The curve moves further up for masses $m_V/3 = m_\chi < m_e$ where only the high velocity tail of the thermal DM population can annihilate into electrons, which needs to be compensated by a larger coupling. However, even though only a small fraction of DM can annihilate into electrons, this is still more efficient than the annihilation into three photons. The latter process, $\chi\chi \rightarrow 3\gamma$ [50,51], was found to be negligible for our study.

The resonance structure seen in all cases arises from resonant mixing of the dark gauge boson V with the SM vector mesons ρ , ω , and ϕ . In the case of DM annihilation, these resonances occur at masses $2m_V/3 = 2m_\chi = m_{\rho,\phi,\omega}$, whereas for V production, these resonances occur at $m_V = m_{\rho,\phi,\omega}$.

D. Existing constraints

Light hadrophilic mediators have a rich phenomenology, giving rise to constraints from previous searches, as well as search opportunities at FPF experiments. Below, we summarize the various laboratory experimental constraints on light hadrophilic gauge bosons following the discussion of Ref. [52]. The resulting limits are shown in Figs. 2 and 3 as dark gray shaded regions.

- (1) Invisible mediator decays: the focus of this study are hadrophilic mediators with a sizable branching

fraction into dark matter. This decay leads to missing energy signatures which have been searched for by various experiments. The most sensitive constraints have been obtained by the search for the decay $\pi^0 \rightarrow \gamma V$ at NA62 [53] and LESB [54]; the search for the decay $\pi^0, \eta, \eta' \rightarrow \gamma V$ at Crystal Barrel [55]; the search for the decay $K^+ \rightarrow \pi^+ V$ at E949 [56] as discussed in Ref. [15,57]; the search for the mixing induced invisible decays of the J/Ψ by BES [58] and the Υ by BaBar [59] as discussed in Ref. [15]; and the monojet search $pp \rightarrow V + \text{jet}$ at CDF [60] as discussed in Ref. [61].

- (2) Visible mediator decays: if the couplings of the hadrophilic mediator to the SM and dark sector have similar size, decays into visible final states are possible. If the coupling is sufficiently large, the decays of the mediator occur promptly in the detector and can be searched for via a bump hunt. Bounds have been obtained by the search for the decay $\eta' \rightarrow V\gamma \rightarrow \pi^0\gamma\gamma$ at GAMS-2000 [62] and the search for the nonelectromagnetic contribution to the decay $\Upsilon(1S) \rightarrow jj$ by ARGUS [63], as discussed in Ref. [64]. In addition, there are bounds from searches for displaced decays of LLPs from NuCAL [65].

- (3) DM and neutrino scattering: the hadrophilic mediator is copiously produced in beam dump experiments. The decay $V \rightarrow \chi\chi^*$ then leads to a dark matter beam. The MiniBooNE collaboration has searched for the scattering of χ in their downstream neutrino detector [66,67]. Recently, even stronger bounds on coherent scatterings of leptophobic DM have been obtained with the coherent CAPTAIN-Mills liquid argon detector [68]. Similarly, the decay $V \rightarrow \nu_\tau \bar{\nu}_\tau$ leads to an increased tau neutrino flux, which can be constrained using measurements from DONuT [69], as discussed in Ref. [52].
- (4) Indirect probes: a hadrophilic mediator can also be constrained indirectly through its contribution to the low-energy neutron-lead scattering cross section [70], as discussed in Ref. [71]. Additionally, a new gauge boson with couplings to tau leptons can be constrained by the measurement of the $Z \rightarrow \tau\tau$ decay width at LEP [72], as discussed in Ref. [73].

In addition, there are other constraints that are somewhat more model dependent. These are the anomaly constraints and the constraints from neutrino NSIs, which are shown as light gray shaded regions in Figs. 2 and 3, and which we now describe:

- (1) Anomaly constraints: as mentioned above, the dark vector boson in the $U(1)_B$ model couples to a nonconserved SM current. Invisible decays of such a vector boson are then constrained by enhanced bounds from missing energy searches in rare Z decays and flavor-changing meson decays $K \rightarrow \pi V$ and $B \rightarrow KV$. We implement them following Refs. [18,19], assuming that anomalies associated with the new gauge group are canceled by heavy fermions that do not receive masses from electroweak symmetry breaking. If these anomalies were canceled by fermions with Yukawa couplings to the Higgs, the invisible decay constraints would not apply, but there would be severe LHC constraints on the additional fermions.
- (2) Neutrino NSI: for the $U(1)_{B-3\tau}$ model, additional constraints arise from studying neutrino oscillations, both in vacuum and in the matter background of the Sun and Earth. These have been precisely measured by a variety of neutrino experiments. A global fit to these neutrino oscillations measurements simultaneously constrains the oscillation parameters and NSI between neutrinos and matter. We present these bounds following Ref. [74].⁴ We note, however, that these constraints are model dependent and could be weakened in the presence of additional new physics.
- (3) Direct detection: further bounds on hadrophilic DM can arise from direct detection (DD) searches [15].

⁴An alternative study, which obtained slightly stronger constraints, was performed in Ref. [75] using the global fit results obtained in Ref. [76].

These, however, depend sensitively on the detailed structure of the DM interaction and do not apply to Majorana DM and to inelastic scalar DM if the mass gap between the dark species is large enough to suppress upscatterings of nonrelativistic DM particles. We stress this in the following when presenting the current DD bounds on spin-independent DM-nuclei scattering from the CRESST-III [77], DarkSide-50 [78], and Xenon 1T [79,80] experiments. We show these bounds assuming that $\Omega_\chi h^2 \simeq 0.12$ [81] in the entire reach plot and that a nonstandard cosmological scenario affects the DM relic density for points in the parameter space away from the thermal target lines.

- (4) Cosmology and astrophysics: further indirect probes arise from possible contributions of light dark vector bosons to the number of relativistic degrees of freedom in the early Universe, ΔN_{eff} . We present them below following Refs. [82,83]. Additional bounds could arise from an enhanced supernova cooling rate of SN1987A, as discussed, for example, in Refs. [84–90]. Such constraints typically probe very small couplings outside the regions of interest for this study. In addition, they are also dependent on a number of astrophysical assumptions, which may weaken the constraints or possibly even remove them altogether; see, e.g., Ref. [91]. In the following, we do not show these bounds explicitly in our sensitivity reach plots, as a detailed study for the models considered here is beyond the scope of our analysis.

III. DETECTORS

We perform our analysis for the on-axis far-forward detectors that will operate either during LHC Run 3 or the HL-LHC era. In the latter case, we focus on the proposed FPF, which begins at a distance $L = 620$ m away from the ATLAS Interaction Point [4]. In particular, we study the expected future sensitivity of the 10-ton emulsion detector FASER ν 2, a proposed successor to the FASER ν experiment that will take data during LHC Run 3 [2,25], as well as the 10- and 100-ton fiducial mass liquid-argon time projection chamber detectors FLArE-10 and FLArE-100 [7]. The relevant detector geometries are

$$\text{FASER}\nu 2: \Delta = 2 \text{ m}, \quad S_T = (0.5 \text{ m} \times 0.5 \text{ m}),$$

$$\text{FLArE-10: } \Delta = 7 \text{ m}, \quad S_T = (1 \text{ m} \times 1 \text{ m}),$$

$$\text{FLArE-100: } \Delta = 30 \text{ m}, \quad S_T = (1.6 \text{ m} \times 1.6 \text{ m}),$$

where Δ is the length of the detector, and S_T denotes its transverse size.

Both types of detectors have excellent capabilities to reconstruct the low-energy nuclear scattering signals created by both neutrinos and hadrophilic DM, and also to disentangle DM-induced events from the more energetic neutrino scatterings. For these searches, however, it is also

important that they be able to reject backgrounds induced by high-energy muons that pass through the facility and interact with the surrounding rock and infrastructure. To veto these muons, it is highly beneficial to collect time information about the events. In the case of FASER ν 2, this would likely require interleaving the emulsion layers with additional electronic detectors. For FLArE, on the other hand, the required time resolution can be more easily obtained by employing an additional light collection system; see Ref. [7] for further discussion.

Throughout this paper, we use the neutrino fluxes for the FPF as presented in Ref. [8]. These fluxes were obtained using the event generator SIBYLL 2.3D [92–95] as implemented in CRMC [96] to simulate the primary collision, and the fast neutrino flux simulation presented in Ref. [97] to model the propagation and decay of long-lived SM hadrons in the forward LHC infrastructure.

In addition to the aforementioned scattering detectors, we will also present sensitivities for the LLP signature of the vector boson mediator decaying to visible SM final states. To this end, we will focus on FASER [24,98] and FASER2, cylindrical detectors with length Δ and radius R , where [6]

$$\text{FASER: } \Delta = 1.5 \text{ m}, \quad R = 10 \text{ cm}, \quad \mathcal{L} = 150 \text{ fb}^{-1},$$

$$\text{FASER2: } \Delta = 5 \text{ m}, \quad R = 1 \text{ m}, \quad \mathcal{L} = 3 \text{ ab}^{-1}.$$

FASER will take data during LHC Run 3 and will be positioned in the far-forward region at a distance $L = 480 \text{ m}$

away from the ATLAS IP. For FASER2 we assume the relevant parameters for the HL-LHC era and the FPF location. Above, we have also provided the relevant integrated luminosities. The multiple collisions that occur in each bunch crossing (pile-up) are accounted for in determining the flux of V .

Throughout the study, we assume perfect detection efficiency for all the events that pass the selection criteria. The probability of passing such criteria depends on the geometrical acceptance of the detectors, energy and other kinematic cuts, as well as on the final state interactions inside the nucleus that we take into account in the case of the elastic scattering. We discuss the relevant cuts for different signatures below.

We will also include in our plots the expected sensitivities of the SND@LHC detector [99] to DM scattering in the $U(1)_B$ model, as determined in Ref. [49]. For the elastic DM scattering signature, this analysis assumed that backgrounds from muon-induced hadrons and photons can be rejected and that the number of neutrino-induced events can also be suppressed to a negligible level. In the DIS regime, the analysis estimated that pure neutrino-induced backgrounds could be reduced to $\mathcal{O}(1000)$ events, and the sensitivity curves were taken to be $N = 100$ DM signal event contours.

IV. SIGNATURES

The hadrophilic models we are considering produce a diverse array of new physics signatures. These are shown in

TABLE I. The signatures studied. In the first three rows, the name of the signature, the subsection in which it is discussed, and the relevant new physics models are given. In the fourth and fifth rows, we show the Feynman diagrams for some example production and detection processes, respectively. The production processes shown are not necessarily the dominant ones. The sixth row shows the dependence of the signal rate on the model parameters, and the seventh row lists the dominant SM backgrounds.

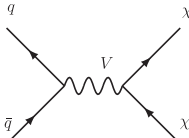
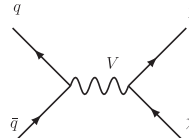
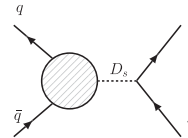
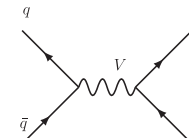
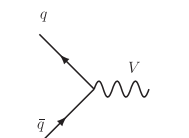
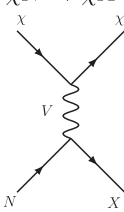
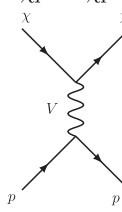
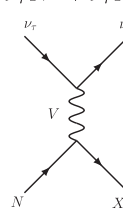
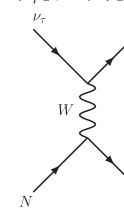
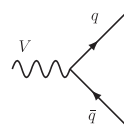
Signature	DM DIS	DM Elastic	ν NC DIS	ν_τ CC DIS	LLP decays
Section	Section IV A	Section IV B	Section IV C	Section IV D	Section IV E
Models	$U(1)_B, U(1)_{B-3\tau}$	$U(1)_B, U(1)_{B-3\tau}$	$U(1)_{B-3\tau}$	$U(1)_{B-3\tau}$	$U(1)_B, U(1)_{B-3\tau}$
Production	$pp \rightarrow V \rightarrow \chi\chi$ 	$pp \rightarrow V \rightarrow \chi\chi$ 	$pp \rightarrow D_s \rightarrow \nu_\tau$ 	$pp \rightarrow V \rightarrow \nu_\tau \bar{\nu}_\tau$ 	$pp \rightarrow V$ 
Detection	$\chi N \rightarrow \chi X$ 	$\chi p \rightarrow \chi p$ 	$\nu_\tau N \rightarrow \nu_\tau X$ 	$\nu_\tau N \rightarrow \tau X$ 	$V \rightarrow \text{hadrons}$ 
Rate scales as	$g_V^6 Q_\chi^2 \sim g_V^4 \alpha_\chi$	$g_V^6 Q_\chi^2 \sim g_V^4 \alpha_\chi$	g_V^4	g_V^2	$g_V^2 e^{-g_V^2 m_V^2}$ or g_V^4
Background	$\nu N \rightarrow \nu X$	$\nu p \rightarrow \nu p$	$\nu N \rightarrow \nu X$	$D_s \rightarrow \nu_\tau \tau$	None

Table I, where we list which models are relevant for each signature, the dominant production and detection processes that determine the signal rates, the dependence of these rates on the model parameters, and the dominant SM backgrounds. As can be seen, the FPF experiments will be sensitive to direct signals generated by both the dark vector boson and DM, as well as to neutrino-induced signals. We now discuss them all in detail.

A. DM deep inelastic scattering

We first consider DM DIS off nuclei, $\chi N \rightarrow \chi X$. At large momentum transfer, DM DIS produces a significant hadronic recoil with multiple charged tracks. The main background is SM neutrino NC interactions. Due to the light mediator, DM scattering prefers lower momentum transfer than the neutrino background, which proceeds through Z-boson exchange. Our discussion of this signature closely follows that in Ref. [8].

The differential cross section for complex scalar DM DIS in the models of Sec. II is given by

$$\begin{aligned} \frac{d\sigma(\chi N \rightarrow \chi X)}{dx dy} &= 4\pi\alpha_\chi\alpha_V \frac{2m_p E_\chi}{(Q^2 + m_{A'}^2)^2} \\ &\times \sum_{q=u,d,s,c} (1-y)[xf_q(x, Q^2) + xf_{\bar{q}}(x, Q^2)], \end{aligned} \quad (16)$$

where x is the parton momentum fraction, $y = 1 - E'_\chi/E_\chi$ is the fraction of the incoming DM energy transferred to the nucleon in the lab frame, $Q^2 = 2m_p E_\chi xy$ is the squared momentum transfer, and f_q is the quark parton distribution function. We use the nCTEQ15 parton distribution functions [100] for tungsten and argon and integrate Eq. (16) requiring $Q^2 > 1 \text{ GeV}^2$ to obtain the expected numbers of DM DIS events in the FPF detectors. We also require the energy transferred to the hadronic system to be $1 \text{ GeV} < E_{\text{had}} < 15 \text{ GeV}$, where $E_{\text{had}} = yE_\chi$, and the total transverse momentum of the recoiling hadrons to be $1 \text{ GeV} < p_{T,\text{had}} < 1.5 \text{ GeV}$, where $p_{T,\text{had}}^2 = Q^2(1-y)$. For the background, we calculate the expected numbers of neutrino NC scattering events satisfying the same cuts on Q^2 , E_{had} , and $p_{T,\text{had}}^2$. Our cuts favor softer hadronic recoils, eliminating much of the neutrino NC background. Our projected sensitivities assume perfect detector efficiency and consider only statistical uncertainties. A previous study [8] of DM DIS at FLArE found that some experimentally motivated cuts did not have a large effect on the signal, but a full study remains to be performed.

B. DM-nucleon elastic scattering

The light DM particles produced in the far-forward region at the LHC can also be discovered via their elastic scatterings with nucleons, which lead to single proton

tracks visible in the detector. We treat this signature following Ref. [8], in which we have also studied the relevant neutrino-induced backgrounds. In particular, when presenting the sensitivity contours, we require the momentum of the outgoing proton to be within the range $300 \text{ MeV} < p_p < 1 \text{ GeV}$ in FASER ν 2, and for FLArE we require $p_p < 1 \text{ GeV}$ and the proton's kinetic energy to satisfy $E_{k,p} > 20 \text{ MeV}$. We also reject events in which other visible tracks emerge from the vertex. After these cuts, we expect ~ 100 , 1000 , and 300 background events during the entire HL-LHC run for FLArE-10, FLArE-100, and FASER ν 2, respectively.

The elastic scattering cross section for the complex scalar DM interacting with the neutron or proton via the hadrophilic gauge boson is

$$\begin{aligned} \frac{d\sigma(\chi p \rightarrow \chi p)}{dQ^2} &= \frac{4\pi\alpha_\chi\alpha_V Q^2}{(E_\chi^2 - m_\chi^2)(m_V^2 + Q^2)^2} \\ &\times \left\{ A(Q^2) + \left(\frac{E_\chi}{Q} - \frac{Q}{4m_N} \right)^2 [(\tilde{F}_{1,N}^B)^2 + \tau(\tilde{F}_{2,N}^B)^2] \right\}, \end{aligned} \quad (17)$$

where $Q^2 = 2m_N(E_N - m_N)$ is the squared four-momentum transfer in terms of the nucleon mass m_N ($N = n, p$) and the outgoing nucleon energy E_N , and E_χ corresponds to the incident DM energy. The term proportional to $A(Q^2)$, which contributes negligibly to the cross section at high energies, is given by

$$A(Q^2) = -\frac{1}{4}(\tilde{F}_{1,N}^B + \tilde{F}_{2,N}^B)^2 \left(\tau + \frac{m_\chi^2}{m_p^2} \right), \quad (18)$$

with $\tau = Q^2/(4m_p^2)$. In contrast to the case of a vanilla dark photon mediator, the neutron and proton form factors are identical in this case and given by

$$\tilde{F}_{1,N}^B(Q^2) = \frac{1 + (\mu_p + \mu_n)\tau}{1 + \tau} G_D(Q^2), \quad (19)$$

$$\tilde{F}_{2,N}^B(Q^2) = \frac{\mu_p + \mu_n - 1}{1 + \tau} G_D(Q^2), \quad (20)$$

where $\mu_p = 2.793$, $\mu_n = -1.913$, and $G_D(Q^2) = (1 + Q^2/M^2)^{-2}$, with $M = 0.843 \text{ GeV}$. The differential elastic scattering cross section becomes form-factor suppressed at large momentum transfers, and the total elastic cross section is dominated by the contribution from $Q^2 \lesssim m_V^2$.

In the following, we include scatterings off both protons and neutrons. For protons, we include the efficiency factors $\sim (50 - 70)\%$ related to the final-state interactions of protons, as in Ref. [8]. For neutrons, we include similar

efficiency factors in the range (15–30)%, which have been obtained as a function of the outgoing neutron momentum by studying neutrino interactions in GENIE [101,102]. In this case, the neutron rescatterings inside the nucleus can lead to an outgoing proton with momentum within the aforementioned cuts and with no other detectable tracks. We find that scatterings of DM off neutrons can contribute up to 25% to the total elastic event rate.

C. Enhanced neutrino neutral current scattering

When a new mediator couples to neutrinos, NC scattering $\nu N \rightarrow \nu X$ receives an additional contribution from the mediator. The signature is identical to that for DM DIS. However, as NC scattering depends only on the couplings of the mediator to quarks and neutrinos, there is no dependence on m_X or Q_X , unlike the case of DM scattering. In particular, for the $B - 3\tau$ mediator, the total ν_τ NC cross section becomes

$$\begin{aligned} \frac{d\sigma(\nu N \rightarrow \nu X)}{dx dy} &= \frac{m_p E_\nu}{4\pi} \sum_{q=u,d,s,c} \{c_L^2 [xf_q(x, Q^2) + x(1-y)^2 f_{\bar{q}}(x, Q^2)] \\ &\quad + c_R^2 [x(1-y)^2 f_q(x, Q^2) + xf_{\bar{q}}(x, Q^2)]\}, \end{aligned} \quad (21)$$

where

$$c_{L/R} = \frac{(g_W g_{\nu,L})(g_W g_{q,L/R})}{\cos^2 \theta_W (Q^2 + m_Z^2)} + \frac{1}{4} \frac{(g_V^2 Q_\nu Q_q)}{(Q^2 + m_V^2)}. \quad (22)$$

Here g_W is the SM weak coupling, $g_{\nu,L} = \frac{1}{2}$, and $g_{q,L} = \frac{1}{2} - \frac{2}{3} \sin^2 \theta_W$ for up-type quarks and $-\frac{1}{2} + \frac{1}{3} \sin^2 \theta_W$ for down-type quarks. The second term in $c_{L,R}$ is the contribution from the new $B - 3\tau$ mediator with charges $Q_\nu = -3$ (3) for ν_τ ($\bar{\nu}_\tau$), and $Q_q = \frac{1}{3}$ for all quarks. The interference term is proportional to $Q_\nu Q_q$, and so carries opposite signs for ν_τ and $\bar{\nu}_\tau$ NC scattering [103]. At the FPF where we expect almost equal fluxes of ν_τ and $\bar{\nu}_\tau$, this implies a small contribution from the interference term after cancellations. Nevertheless we use the complete expression above in our analysis.

For small m_V , the BSM contribution to NC scattering prefers low recoil energy, similar to DM DIS and unlike the weak boson-mediated SM process, whose cross section grows with momentum transfer. We calculate the number of additional NC events expected at the FPF with Eq. (21), using the same parton distribution functions and minimum Q^2 cut as in Sec. IV A. Because of the small relative flux of tau neutrinos compared to muon and electron neutrinos, the impact of the light mediator on the total NC cross section must be significant to provide a sizable effect relative to the SM NC background.

In testing whether an excess of NC events is observable, we consider only statistical uncertainties and neglect systematic uncertainties. For simplicity, we also assume perfect detection efficiency for NC interactions; the inclusion of realistic detection efficiencies [104] would not substantially change the positions of the limits from excess NC events in Figs. 2 and 3, relative to the other signatures that we consider. We note that the main systematic uncertainty in the NC cross section measurement, the neutrino flux, can be constrained by measurements of charged current (CC) interactions. We find a statistically significant effect from the BSM contribution to NC scattering when the coupling to mass ratio of the new interaction is comparable to that of the weak interaction, $g_V/m_V \gtrsim g_W/m_W \approx 10^{-2} \text{ GeV}^{-1}$.

D. Excess of tau neutrino flux

In the case of the gauged $B - 3\tau$ scenario, the hadrophilic mediator decays into tau neutrinos with a sizable branching fraction.⁵ As discussed in Ref. [52], this opens another opportunity to probe this model via their contribution to the LHC tau neutrino flux. In the SM, tau neutrinos are mainly produced via $D_s \rightarrow \nu_\tau$ and subsequent τ decays, which occurs in roughly one in 10^5 collisions at the LHC. This means that even rare BSM processes could lead to sizable contributions to the tau neutrino flux. The relevant detection channel in this case is via ν_τ CC scatterings off nuclei. The displaced decays of the outgoing boosted tau lepton must then be identified in the detector, requiring excellent spatial resolution.

An important issue that arises when searching for signs of new physics is the large uncertainty on the normalization of the SM tau neutrino flux [97,105]. Although future efforts are expected to reduce these uncertainties, we will follow a different approach. In contrast to tau neutrinos from charm and tau decays, which have a broader angular spread, tau neutrinos from light mediator decays are more centered around the beam collision axis. In this study, we use this feature and perform a shape analysis of the ν_τ angular distribution, which does not rely on knowledge of the neutrino flux normalization. We focus on the FLArE-10 design, whose $1 \text{ m} \times 1 \text{ m}$ cross sectional area is sufficiently large to capture this effect. More precisely, we define five concentric rectangular bins centered around the beam collision axis and corresponding to the distance between d and $d + 10 \text{ cm}$ away from it, where $d = 0, 10, 20, 30, 40 \text{ cm}$. In practice, the most important contribution to the BSM-induced excess of ν_τ s is from the two most central bins, i.e., at distances up to $d \lesssim 20 \text{ cm}$ away from the beam collision axis.

⁵Additional ν_τ flux can be produced via V decays into tau leptons for $m_V \gtrsim 2m_\tau$. However, the corresponding expected sensitivity lies in a region of parameter space that is already excluded, as shown in Sec. V.

E. Visible decays of the dark vector boson

In the following, we study the decay signature using the FORESEE package [41] with the lifetimes modeled with DARKCAST [45] and the spectrum of light hadrons obtained from EPOS-LHC [106]. We assume 100% detection efficiency for all visible final states. We present the results for both FASER and FASER2. In the analysis, we require the total energy of the visible products of the vector boson decays to be at least 100 GeV. This cut has a minor impact on the BSM signal events, but suppresses possible SM backgrounds to a negligible level [24,98]. Visibly decaying dark vector bosons could also appear in secondary production processes due to DM scatterings occurring right in front of or even inside the detector [107]. We neglect the impact of such processes below, as we do not expect them to improve the sensitivity reach of the FPF detectors in the models under study.

V. RESULTS

In Fig. 2, we present the results of our analysis for both the $U(1)_B$ and $U(1)_{B-3\tau}$ models in the (m_V, g_V) plane. In the plots, we fix the DM coupling to $\alpha_\chi = 0.01$ and 0.5 in the upper and lower panels, respectively, and we keep a constant mass ratio between the dark sector particles, $m_V = 3m_\chi$. In dark gray, we show the existing constraints, as discussed in Sec. II D, while the black solid (dashed) lines correspond to the relic density targets for the complex scalar (Majorana) DM. We stress that, although the anomaly bounds, shown in light gray in the left panels for the $U(1)_B$ case, can be avoided in modified versions of this simplified scenario, this often leads to further constraints due to additional couplings of the dark vector bosons that are introduced in the model to make it anomaly free. An example is shown in the right panels for the anomaly-free $U(1)_{B-3\tau}$ model, where the NSI constraints cover a good portion of the parameter space shown in the plot.

In Fig. 2, we also present the expected 90% confidence limits (C.L.) exclusion bounds in searches for DM scatterings off nuclei in the elastic (dark red) and DIS (light red) channels for FLArE-10 (solid), FLArE-100 (dash-dotted), and FASER ν 2 (dotted). As is clear from the plot, the elastic scattering probe is stronger for light DM and mediator masses below 1 GeV, which favor interactions with low momentum exchange. For $m_V \gtrsim 1$ GeV, the elastic scattering rate is suppressed by the form factor and the cut on the outgoing proton momentum $p_p \lesssim 1$ GeV. In this higher mass range, the search based on DIS processes provides the best reach. For comparison, we also show the expected reach of the SND@LHC detector [49] with the assumptions noted in Sec. III.

For the $U(1)_B$ model with fixed $\alpha_\chi = 0.01$ shown in the upper left panel of Fig. 2, we expect that future searches at the FPF will cover almost the entire remaining allowed

region in the parameter space above the Majorana and complex scalar relic target lines, in which DM is not thermally overproduced in the early Universe. This corresponds to vector boson masses between 1 and 3 GeV. For the simple complex scalar DM model, additional stringent bounds for $m_\chi \gtrsim 200$ MeV can arise from past DM DD searches, which are indicated in the plots by the very light gray shaded regions and cover the region within the sensitivity of FLArE and FASER ν 2. However, these limits can be evaded in the inelastic scalar DM case and are not relevant for Majorana DM. For lower masses, (a few) MeV $\lesssim m_V \lesssim 1$ GeV, the expected FLArE and FASER ν 2 bounds extend beyond current constraints from the coherent CAPTAIN-Mills, MiniBooNE, and NA62 experiments. Here, the searches at the FPF would probe regions in the parameter space that are otherwise partially excluded only by anomaly-induced rare K and Z decays.

Next, we consider the $U(1)_{B-3\tau}$ model with fixed $\alpha_\chi = 0.01$ shown in the upper right panel of Fig. 2. Since the model is free of gauge anomalies, the stringent constraints from rare Z and meson decays present in the $U(1)_B$ model are absent in this case. On the other hand, the additional bounds from neutrino NSI cover much of the model parameter space. Nevertheless, we observe that the FPF detectors can still explore a portion of the currently allowed parameter space, especially in the ω and ϕ resonance regions, $m_V \sim m_\omega, m_\phi$, and the corresponding part of the relic target line for complex scalar DM. In this model, additional sensitivity arises from dark vector boson-mediated scattering of tau neutrinos in the DIS regime; see Sec. IV C. The relevant expected bounds, which are indicated by the light purple lines in the plots, impact parameter regions that are already excluded by past searches. We note that the actual exclusion bound in the DIS channel should be derived using the combined excess signal rates for both DM and BSM neutrino scatterings over the expected SM backgrounds. Instead, in the plot, we have presented the expected bounds for each separately to allow for independent discussion of the impact of different new physics effects.

For larger values of α_χ , the relic target lines shift downwards relative to the FPF sensitivity contours from DM scattering. This is dictated by the different parametric dependence of the annihilation cross section and the number of DM scattering events in the FPF experiments on the coupling constants, $\langle\sigma v\rangle \sim g_V^2 \alpha_\chi$ and $N_{\text{ev}} \sim g_V^4 \alpha_\chi$, respectively. As a result, in the lower panel of Fig. 2 obtained for $\alpha_\chi = 0.5$, we observe that both FLArE and FASER ν 2 will only partially cover the thermal target lines for the $U(1)_B$ model. Instead, in the $U(1)_{B-3\tau}$ case, they will typically probe regions in the parameter space predicting subdominant fractions of thermally produced χ DM.

Thus far we have considered scenarios in which the vector boson mediator couples much more strongly to DM than to SM particles, $Q_\chi \gg 1$. In Fig. 3 we consider the

different scenario in which the vector boson mediator couples with comparable strength to complex scalar DM and SM particles, with Q_χ fixed according to Eq. (9). As can be seen, for both the $U(1)_B$ and $U(1)_{B-3\tau}$ models, FLArE-10 can cover the entire relic target line in a wide vector boson mass range between 1 MeV and 10 GeV. As in the previous scenarios depicted in Fig. 2, significant portions of these regions are already constrained by either anomaly-induced or NSI bounds, as well as by the other past searches indicated in the plots. However, we emphasize that for the case of inelastic scalar DM in the $U(1)_B$ model, to which DD constraints do not apply, FLArE-10 will be able to test an interesting open region of parameter space for vector boson mass of order several GeV that is consistent with the observed DM abundance.

Figure 3 also highlights the rich phenomenology present in scenarios with comparable DM and SM couplings to the vector boson mediator. Along with the scattering searches relevant for DM and BSM neutrino interactions, additional prospects arise at very small couplings from FPF searches for visible decays of the long-lived vector boson mediator; see Sec. II B. In particular, for m_V between several hundred MeV and a GeV and coupling $10^{-8} \lesssim g_V \lesssim 10^{-5}$, such displaced decays into visible final states, primarily light hadrons, can be detected at both FASER and FASER2. The dominant branching fraction in this case is into three pions, $\pi^0 \pi^+ \pi^-$, which leads to a striking signature consisting of a photon pair accompanied by two oppositely charged tracks.

We present the relevant expected 90% C.L. exclusion bounds on LLP decays for FASER (dark blue) and FASER2 (light blue) in the plots. These correspond to the region of parameter space with $m_V \sim m_\omega$ or m_ϕ . Here, both the dark vector boson production via proton bremsstrahlung and its decay branching fractions into light hadrons are enhanced. The expected exclusions shown in the plot are bounded from below by the production rate of the dark vector bosons being too low, and from above by the V lifetime being too small for the boson to decay in the detectors. In the $U(1)_B$ model, further sensitivity at FPF experiments can be obtained for $m_V \lesssim 10$ MeV due to loop-induced dark vector boson decay into an $e^+ e^-$ pair. This scenario is, however, already constrained by the past beam-dump search in NuCal and by the anomaly-induced bounds.

Last but not least, in the $U(1)_{B-3\tau}$ model, further constraints arise due to the dominant dark vector boson decays into tau neutrinos. These can generate an excess flux of ν_τ s over the expected SM production rates, which can be detected via their CC scatterings in the detector, as described in Sec. IV D. The corresponding expected sensitivity is indicated by the green contour in the right panel of Fig. 3. For $m_V \lesssim 2$ GeV, this sensitivity is greater than from the DM and BSM neutrino searches. In particular, it allows one to constrain the currently allowed region of the parameter space of the model close to the ω - and

ϕ -resonance regions. In this case, the increased flux of ν_τ s could also further contribute to the aforementioned NC DIS signal rate due to BSM tau neutrino interactions. To isolate the impact of various new physics effects, we do not take this into account when presenting relevant expected bounds, which should thus be considered conservative. We stress that the dominant expected bound in the corresponding region of the parameter space is, in any case, due to excess CC ν_τ scatterings.

VI. CONCLUSIONS

While the ability of the LHC to search for TeV-scale DM is well known, recently proposed dedicated experiments at high rapidity can significantly enhance the potential of the LHC to probe light DM. Beyond the minimal portal extensions of the SM that allow for light DM and an associated mediator, new gauge groups represent a well-motivated class of possible dark sector models. In this paper, we have explored the use of the FPF to study such $U(1)$ theories leading to hadrophilic dark sectors. In particular, these remain beyond the reach of experiments focusing on BSM electron couplings, while they can more straightforwardly be studied at the LHC.

The suite of FPF experiments provides a comprehensive set of tests of these theories in different regions of parameter space. DM produced in pp collisions can scatter in the FASER ν 2 and FLArE detectors through the new light vector boson; we have considered both elastic and deep inelastic scattering. Furthermore, if the mediator has a significant decay branching ratio to SM states, the FASER2 LLP detector can search for the visible decay products. In fact, already at Run 3, the FASER detector will begin to test hadrophilic $U(1)$ theories at couplings substantially lower than existing bounds. These hadrophilic models therefore motivate near-term searches at FASER for new LLP signatures

$$V \rightarrow \pi^0 \gamma, \quad \pi^+ \pi^- \pi^0, \quad K^+ K^-, \quad K_S K_L, \quad (23)$$

which are not motivated by dark photon models for FASER in Run 3. Finally, if neutrinos are also charged under the new gauge symmetry, additional signatures are possible in the scattering detectors. We have demonstrated that with a symmetry under which tau neutrinos are charged, the ν_τ flux and NC cross section are both enhanced, leading to potential deviations in ν_τ CC and NC scattering rates.

These results for $U(1)_B$ and $U(1)_{B-3\tau}$ models should be considered as illustrative of the complementarity of forward LHC experiments in searching for light dark sectors, particularly between LLP and scattering detectors. In both of these theories, the FPF can test broad regions in the coupling-gauge boson mass plane, including significant expanses over which the observed DM relic density could be obtained through standard thermal freeze-out. For our benchmark scenario with scalar DM, $m_V = 3m_\chi$ and low

values of the dark charge Q_χ given by Eq. (9), FPF searches can probe well below the thermal relic target lines in each model for nearly all gauge boson masses between 1 MeV and 10 GeV. Throughout our results, the strongest searches tend to be those based on DM elastic scattering and DIS, with distinct additional reach possible from LLP searches when the mediator can decay to SM final states. For the $B - 3\tau$ model, searches for an increased ν_τ flux would also test new space.

The models that we have studied face strong indirect constraints, notably from rare invisible decays and neutrino oscillations, but we emphasize that FPF searches can test couplings that are smaller than these formidable existing bounds. In addition, in the GeV mass range, these searches provide constraints that are complementary to those from spin-independent DD, the latter only being applicable in the case of elastic scalar DM.

Though we have chosen to focus on two possible gauge groups with a handful of coupling and mass assumptions, the general interplay between the DM scattering, LLP and neutrino searches is likely to persist for other theories and parameter choices. To determine the gain provided by the FPF in a particular theory, the reach of these searches must be compared against those from other bounds. As we have seen, U(1) theories that are not anomaly free typically face rare meson decay constraints, while those with nonzero lepton charges can encounter NSI bounds. For models with couplings to first and second generation leptons, additional limits from beam dump and neutrino experiments would likely need to be considered as well.

Forward LHC detectors offer a distinct perspective on light hidden sectors, allowing for searches for light DM and its associated mediators in an otherwise inaccessible kinematic regime. The results here underscore the utility of different types of forward detectors, as could be provided at the FPF. The multipronged approach to uncovering physics beyond the SM that is enabled by such a facility,

along with other uses such as measurements of SM neutrino interactions and tests of QCD, bolsters the physics case for the FPF.

ACKNOWLEDGMENTS

We thank Daniele Alves, Asher Berlin, Patrick deNiverville, Peter Reimitz, and Tyler Thornton for useful discussions and correspondence. We are also grateful to the authors and maintainers of many open-source software packages, including FEYNALC [108], GENIE [101,102], LHAPDF [109], and SCIKIT-HEP [110]. The work of B. B. is supported by the U.S. Department of Energy (DOE) under Grant No. DESC0007914. The work of J. L. F. is supported in part by U.S. National Science Foundation (NSF) Grants No. PHY-1915005 and No. PHY-2111427 and by Simons Investigator Award #376204. M. F. is supported in part by NSF Grant No. PHY-1915005 and by NSF Graduate Research Fellowship Award No. DGE-1839285. A. I. and R. M. A. are supported in part by the DOE under Grant No. DE-SC0016013. R. M. A. is supported in part by the Dr. Swamy Memorial Scholarship. The work of F. K. is supported by the DOE under Grant No. DE-AC02-76SF00515 and by the Deutsche Forschungsgemeinschaft under Germany's Excellence Strategy—EXC 2121 Quantum Universe—Grant No. 390833306. S. T. is supported by the grant “AstroCeNT: Particle Astrophysics Science and Technology Centre” carried out within the International Research Agendas programme of the Foundation for Polish Science financed by the European Union under the European Regional Development Fund. S. T. is supported in part by the Polish Ministry of Science and Higher Education through its scholarship for young and outstanding scientists (Decision No. 1190/E-78/STYP/14/2019). S. T. is also supported in part from the European Unions Horizon 2020 research and innovation program under Grant Agreement No. 952480 (DarkWave project).

-
- [1] H. Abreu *et al.* (FASER Collaboration), First neutrino interaction candidates at the LHC, *Phys. Rev. D* **104**, L091101 (2021).
 - [2] H. Abreu *et al.* (FASER Collaboration), Detecting and studying high-energy collider neutrinos with FASER at the LHC, *Eur. Phys. J. C* **80**, 61 (2020).
 - [3] C. Ahdida *et al.* (SHiP Collaboration), SND@LHC, *arXiv*:2002.08722.
 - [4] L. A. Anchordoqui *et al.*, The forward physics facility: Sites, experiments, and physics potential, *arXiv*:2109.10905.
 - [5] J. L. Feng, I. Galon, F. Kling, and S. Trojanowski, Forward search experiment at the LHC, *Phys. Rev. D* **97**, 035001 (2018).
 - [6] A. Ariga *et al.* (FASER Collaboration), FASER's physics reach for long-lived particles, *Phys. Rev. D* **99**, 095011 (2019).
 - [7] B. Batell, J. L. Feng, and S. Trojanowski, Detecting dark matter with far-forward emulsion and liquid argon detectors at the LHC, *Phys. Rev. D* **103**, 075023 (2021).
 - [8] B. Batell, J. L. Feng, A. Ismail, F. Kling, R. M. Abraham, and S. Trojanowski, Discovering dark matter at the LHC through its nuclear scattering in far-forward emulsion and liquid argon detectors, *Phys. Rev. D* **104**, 035036 (2021).
 - [9] W. Altmannshofer *et al.* (Belle-II Collaboration), The Belle II physics book, *Prog. Theor. Exp. Phys.* **2019**, 123C01 (2019); **2020**, 029201(E) (2020).

- [10] D. Banerjee (NA64, Physics Beyond Colliders Conventional Beams Working Group Collaboration), Search for dark sector physics at the NA64 experiment in the context of the physics beyond colliders projects, *Proc. Sci. LeptonPhoton2019* (**2019**) 061 [[arXiv:1909.04363](#)].
- [11] T. Åkesson *et al.* (LDMX Collaboration), Light dark matter experiment (LDMX), [arXiv:1808.05219](#).
- [12] J. Tiffenberg, M. Sofo-Haro, A. Drlica-Wagner, R. Essig, Y. Guardincerri, S. Holland, T. Volansky, and T.-T. Yu (SENSEI Collaboration), Single-Electron and Single-Photon Sensitivity with a Silicon Skipper CCD, *Phys. Rev. Lett.* **119**, 131802 (2017).
- [13] B. A. Dobrescu and C. Frugiuale, Hidden GeV-scale interactions of quarks, *Phys. Rev. Lett.* **113**, 061801 (2014).
- [14] S. Tulin, New weakly-coupled forces hidden in low-energy QCD, *Phys. Rev. D* **89**, 114008 (2014).
- [15] B. Batell, P. deNiverville, D. McKeen, M. Pospelov, and A. Ritz, Leptophobic dark matter at neutrino factories, *Phys. Rev. D* **90**, 115014 (2014).
- [16] D. E. Soper, M. Spannowsky, C. J. Wallace, and T. M. P. Tait, Scattering of dark particles with light mediators, *Phys. Rev. D* **90**, 115005 (2014).
- [17] B. A. Dobrescu and C. Frugiuale, GeV-scale dark matter: Production at the main injector, *J. High Energy Phys.* **02** (2015) 019.
- [18] J. A. Dror, R. Lasenby, and M. Pospelov, New Constraints on Light Vectors Coupled to Anomalous Currents, *Phys. Rev. Lett.* **119**, 141803 (2017).
- [19] J. A. Dror, R. Lasenby, and M. Pospelov, Dark forces coupled to nonconserved currents, *Phys. Rev. D* **96**, 075036 (2017).
- [20] P. Fileviez Perez and M. B. Wise, Baryon and lepton number as local gauge symmetries, *Phys. Rev. D* **82**, 011901 (2010); **82**, 079901(E) (2010).
- [21] M. Duerr, P. Fileviez Perez, and M. B. Wise, Gauge Theory for Baryon and Lepton Numbers with Leptoquarks, *Phys. Rev. Lett.* **110**, 231801 (2013).
- [22] M. Duerr and P. Fileviez Perez, Baryonic dark matter, *Phys. Lett. B* **732**, 101 (2014).
- [23] P. Fileviez Perez, S. Ohmer, and H. H. Patel, Minimal theory for lepto-baryons, *Phys. Lett. B* **735**, 283 (2014).
- [24] A. Ariga *et al.* (FASER Collaboration), Technical proposal for FASER: Forward search experiment at the LHC, [arXiv:1812.09139](#).
- [25] H. Abreu *et al.* (FASER Collaboration), Technical proposal: FASERnu, [arXiv:2001.03073](#).
- [26] C. Ahdida *et al.* (SND@LHC Collaboration), SND@LHC—Scattering and Neutrino Detector at the LHC, CERN Technical Report No. CERN-LHCC-2021-003; LHCC-P-016, 2021.
- [27] A. Haas, C. S. Hill, E. Izaguirre, and I. Yavin, Looking for milli-charged particles with a new experiment at the LHC, *Phys. Lett. B* **746**, 117 (2015).
- [28] S. Foroughi-Abari, F. Kling, and Y.-D. Tsai, Looking forward to millicharged dark sectors at the LHC, *Phys. Rev. D* **104**, 035014 (2021).
- [29] J. L. Feng, F. Kling *et al.*, Forward physics facility: Snowmass 2021 letter of interest, [10.5281/zenodo.4009640](#) (2020).
- [30] K. Jodłowski and S. Trojanowski, Neutrino beam-dump experiment with FASER at the LHC, *J. High Energy Phys.* **05** (2021) 191.
- [31] P. A. R. Ade *et al.* (Planck Collaboration), Planck 2015 results. XIII. Cosmological parameters, *Astron. Astrophys.* **594**, A13 (2016).
- [32] T. R. Slatyer, N. Padmanabhan, and D. P. Finkbeiner, CMB constraints on WIMP annihilation: Energy absorption during the recombination epoch, *Phys. Rev. D* **80**, 043526 (2009).
- [33] T. Han and R. Hempfling, Messenger sneutrinos as cold dark matter, *Phys. Lett. B* **415**, 161 (1997).
- [34] L. J. Hall, T. Moroi, and H. Murayama, Sneutrino cold dark matter with lepton number violation, *Phys. Lett. B* **424**, 305 (1998).
- [35] D. Tucker-Smith and N. Weiner, Inelastic dark matter, *Phys. Rev. D* **64**, 043502 (2001).
- [36] M. Bauer, P. Foldenauer, and J. Jaeckel, Hunting all the hidden photons, *J. High Energy Phys.* **07** (2018) 094.
- [37] A. Berlin, N. Blinov, G. Krnjaic, P. Schuster, and N. Toro, Dark matter, millicharges, axion and scalar particles, gauge bosons, and other new physics with LDMX, *Phys. Rev. D* **99**, 075001 (2019).
- [38] B. Batell, A. Freitas, A. Ismail, and D. McKeen, Flavor-specific scalar mediators, *Phys. Rev. D* **98**, 055026 (2018).
- [39] B. Batell, A. Freitas, A. Ismail, and D. McKeen, Probing light dark matter with a hadrophilic scalar mediator, *Phys. Rev. D* **100**, 095020 (2019).
- [40] B. Batell, A. Freitas, A. Ismail, D. McKeen, and M. Rai, Renormalizable models of flavor-specific scalars, *Phys. Rev. D* **104**, 115032 (2021).
- [41] F. Kling and S. Trojanowski, Forward experiment sensitivity estimator for the LHC and future hadron colliders, *Phys. Rev. D* **104**, 035012 (2021).
- [42] J. Blümlein and J. Brunner, New exclusion limits on dark gauge forces from proton bremsstrahlung in beam-dump data, *Phys. Lett. B* **731**, 320 (2014).
- [43] P. deNiverville, C.-Y. Chen, M. Pospelov, and A. Ritz, Light dark matter in neutrino beams: Production modelling and scattering signatures at MiniBooNE, T2K and SHiP, *Phys. Rev. D* **95**, 035006 (2017).
- [44] S. Foroughi-Abari and A. Ritz, Dark sector production via proton bremsstrahlung, [arXiv:2108.05900](#).
- [45] P. Ilten, Y. Soreq, M. Williams, and W. Xue, Serendipity in dark photon searches, *J. High Energy Phys.* **06** (2018) 004.
- [46] T. Plehn, P. Reimitz, and P. Richardson, Hadronic footprint of GeV-mass dark matter, *SciPost Phys.* **8**, 092 (2020).
- [47] P. Gondolo and G. Gelmini, Cosmic abundances of stable particles: Improved analysis, *Nucl. Phys. B* **360**, 145 (1991).
- [48] G. Steigman, B. Dasgupta, and J. F. Beacom, Precise relic WIMP abundance and its impact on searches for dark matter annihilation, *Phys. Rev. D* **86**, 023506 (2012).
- [49] A. Boyarsky, O. Mikulenko, M. Ovchinnikov, and L. Shchutska, Searches for new physics at SND@LHC, *J. High Energy Phys.* **03** (2022) 006.
- [50] M. Pospelov, A. Ritz, and M. B. Voloshin, Bosonic super-WIMPs as keV-scale dark matter, *Phys. Rev. D* **78**, 115012 (2008).

- [51] S. D. McDermott, H. H. Patel, and H. Ramani, Dark photon decay beyond the Euler-Heisenberg limit, *Phys. Rev. D* **97**, 073005 (2018).
- [52] F. Kling, Probing light gauge bosons in tau neutrino experiments, *Phys. Rev. D* **102**, 015007 (2020).
- [53] E. C. Gil *et al.*, Search for production of an invisible dark photon in π^0 decays, *J. High Energy Phys.* **05** (2019) 182.
- [54] M. S. Atiya *et al.*, Search for the Decay $\pi^0 \rightarrow \gamma X$, *Phys. Rev. Lett.* **69**, 733 (1992).
- [55] C. Amsler *et al.*, Search for a new light gauge boson in decays of π^0 and η , *Phys. Lett. B* **333**, 271 (1994).
- [56] A. V. Artamonov *et al.*, Study of the decay $K^+ \rightarrow \pi^+ \nu \bar{\nu}$ in the momentum region $140 < P_\pi < 199$ MeV/c, *Phys. Rev. D* **79**, 092004 (2009).
- [57] M. Pospelov, Secluded U(1) below the weak scale, *Phys. Rev. D* **80**, 095002 (2009).
- [58] M. Ablikim *et al.* (BES Collaboration), Search for the Invisible Decay of J/ψ in $\psi(2S) \rightarrow \pi^+ \pi^- J/\psi$, *Phys. Rev. Lett.* **100**, 192001 (2008).
- [59] B. Aubert *et al.* (BaBar Collaboration), A Search for Invisible Decays of the Upsilon(1S), *Phys. Rev. Lett.* **103**, 251801 (2009).
- [60] T. Aaltonen *et al.*, A Search for Dark Matter in Events with One Jet and Missing Transverse Energy in $p\bar{p}$ collisions at $\sqrt{s} = 1.96$ TeV, *Phys. Rev. Lett.* **108**, 211804 (2012).
- [61] I. M. Shoemaker and L. Vecchi, Unitarity and monojet bounds on models for DAMA, CoGeNT, and CRESST-II, *Phys. Rev. D* **86**, 015023 (2012).
- [62] D. Alde *et al.* (Serpukhov-Brussels-Los Alamos-Annecy (LAPP) Collaboration), Neutral decays of η' (958), *Z. Phys. C* **36**, 603 (1987).
- [63] H. Albrecht *et al.* (ARGUS Collaboration), An upper limit for two jet production in direct Υ (1s) decays, *Z. Phys. C* **31**, 181 (1986).
- [64] A. Aranda and C. D. Carone, Limits on a light leptophobic gauge boson, *Phys. Lett. B* **443**, 352 (1998).
- [65] J. Blumlein *et al.*, Limits on neutral light scalar and pseudoscalar particles in a proton beam dump experiment, *Z. Phys. C* **51**, 341 (1991).
- [66] A. A. Aguilar-Arevalo *et al.* (MiniBooNE Collaboration), Dark Matter Search in a Proton Beam Dump with MiniBooNE, *Phys. Rev. Lett.* **118**, 221803 (2017).
- [67] A. A. Aguilar-Arevalo *et al.* (MiniBooNE DM Collaboration), Dark matter search in nucleon, pion, and electron channels from a proton beam dump with MiniBooNE, *Phys. Rev. D* **98**, 112004 (2018).
- [68] A. A. Aguilar-Arevalo *et al.*, First leptophobic dark matter search from Coherent CAPTAIN-Mills, [arXiv:2109.14146](https://arxiv.org/abs/2109.14146).
- [69] K. Kodama *et al.* (DONuT Collaboration), Final tau-neutrino results from the DONuT experiment, *Phys. Rev. D* **78**, 052002 (2008).
- [70] R. Barbieri and T. E. O. Ericson, Evidence against the existence of a low mass scalar boson from neutron-nucleus scattering, *Phys. Lett.* **57B**, 270 (1975).
- [71] V. Barger, C.-W. Chiang, W.-Y. Keung, and D. Marfatia, Proton Size Anomaly, *Phys. Rev. Lett.* **106**, 153001 (2011).
- [72] M. Tanabashi *et al.* (Particle Data Group), Review of particle physics, *Phys. Rev. D* **98**, 030001 (2018).
- [73] E. Ma and D. Roy, Phenomenology of the $B-3L(\tau)$ gauge boson, *Phys. Rev. D* **58**, 095005 (1998).
- [74] T. Han, J. Liao, H. Liu, and D. Marfatia, Nonstandard neutrino interactions at COHERENT, DUNE, T2HK and LHC, *J. High Energy Phys.* **11** (2019) 028.
- [75] J. Heeck, M. Lindner, W. Rodejohann, and S. Vogl, Non-standard neutrino interactions and neutral gauge bosons, *SciPost Phys.* **6**, 038 (2019).
- [76] I. Esteban, M. Gonzalez-Garcia, M. Maltoni, I. Martinez-Soler, and J. Salvado, Updated constraints on non-standard interactions from global analysis of oscillation data, *J. High Energy Phys.* **08** (2018) 180.
- [77] A. H. Abdelhameed *et al.* (CRESST Collaboration), First results from the CRESST-III low-mass dark matter program, *Phys. Rev. D* **100**, 102002 (2019).
- [78] P. Agnes *et al.* (DarkSide Collaboration), Low-Mass Dark Matter Search with the Darkside-50 Experiment, *Phys. Rev. Lett.* **121**, 081307 (2018).
- [79] E. Aprile *et al.* (XENON Collaboration), Dark Matter Search Results from a One Ton-Year Exposure of XENON1T, *Phys. Rev. Lett.* **121**, 111302 (2018).
- [80] E. Aprile *et al.* (XENON Collaboration), Search for Coherent Elastic Scattering of Solar ^8B Neutrinos in the XENON1T Dark Matter Experiment, *Phys. Rev. Lett.* **126**, 091301 (2021).
- [81] N. Aghanim *et al.* (Planck Collaboration), Planck 2018 results. VI. Cosmological parameters, *Astron. Astrophys.* **641**, A6 (2020); **652**, C4(E) (2021).
- [82] M. Escudero, D. Hooper, G. Krnjaic, and M. Pierre, Cosmology with a very light $L_\mu - L_\tau$ gauge boson, *J. High Energy Phys.* **03** (2019) 071.
- [83] M. Bauer, P. Foldenauer, and M. Mosny, Flavor structure of anomaly-free hidden photon models, *Phys. Rev. D* **103**, 075024 (2021).
- [84] J. B. Dent, F. Ferrer, and L. M. Krauss, Constraints on light hidden sector gauge bosons from supernova cooling, [arXiv:1201.2683](https://arxiv.org/abs/1201.2683).
- [85] H. K. Dreiner, J.-F. Fortin, C. Hanhart, and L. Ubaldi, Supernova constraints on MeV dark sectors from e^+e^- annihilations, *Phys. Rev. D* **89**, 105015 (2014).
- [86] D. Kazanas, R. N. Mohapatra, S. Nussinov, V. L. Teplitz, and Y. Zhang, Supernova bounds on the dark photon using its electromagnetic decay, *Nucl. Phys.* **B890**, 17 (2014).
- [87] E. Rrapaj and S. Reddy, Nucleon-nucleon bremsstrahlung of dark gauge bosons and revised supernova constraints, *Phys. Rev. C* **94**, 045805 (2016).
- [88] J. H. Chang, R. Essig, and S. D. McDermott, Revisiting supernova 1987A constraints on dark photons, *J. High Energy Phys.* **01** (2017) 107.
- [89] J. H. Chang, R. Essig, and S. D. McDermott, Supernova 1987A constraints on sub-GeV dark sectors, millicharged particles, the QCD axion, and an axion-like particle, *J. High Energy Phys.* **09** (2018) 051.
- [90] A. Sung, H. Tu, and M.-R. Wu, New constraint from supernova explosions on light particles beyond the Standard Model, *Phys. Rev. D* **99**, 121305 (2019).
- [91] N. Bar, K. Blum, and G. D'Amico, Is there a supernova bound on axions?, *Phys. Rev. D* **101**, 123025 (2020).

- [92] E.-J. Ahn, R. Engel, T. K. Gaisser, P. Lipari, and T. Stanev, Cosmic ray interaction event generator SIBYLL 2.1, *Phys. Rev. D* **80**, 094003 (2009).
- [93] F. Riehn, R. Engel, A. Fedynitch, T. K. Gaisser, and T. Stanev, A new version of the event generator Sibyll, *Proc. Sci. ICRC2015* (2016) 558 [[arXiv:1510.00568](#)].
- [94] F. Riehn, H. P. Dembinski, R. Engel, A. Fedynitch, T. K. Gaisser, and T. Stanev, The hadronic interaction model SIBYLL 2.3c and Feynman scaling, *Proc. Sci. ICRC2017* (2018) 301 [[arXiv:1709.07227](#)].
- [95] F. Riehn, R. Engel, A. Fedynitch, T. K. Gaisser, and T. Stanev, Hadronic interaction model Sibyll 2.3d and extensive air showers, *Phys. Rev. D* **102**, 063002 (2020).
- [96] C. Baus, T. Pierog, and R. Ulrich, Cosmic Ray Monte Carlo (CRMC), <https://web.ikp.kit.edu/rulrich/crmc.html>.
- [97] F. Kling, Forward neutrino fluxes at the LHC, *Phys. Rev. D* **104**, 113008 (2021).
- [98] A. Ariga *et al.* (FASER Collaboration), Letter of intent for FASER: ForwArd Search ExpeRiment at the LHC, [arXiv:1811.10243](#).
- [99] C. Ahdida *et al.* (SHiP Collaboration), SND@LHC, [arXiv:2002.08722](#).
- [100] K. Kovarik *et al.*, nCTEQ15—Global analysis of nuclear parton distributions with uncertainties in the CTEQ framework, *Phys. Rev. D* **93**, 085037 (2016).
- [101] C. Andreopoulos *et al.*, The GENIE neutrino Monte Carlo generator, *Nucl. Instrum. Methods Phys. Res., Sect. A* **614**, 87 (2010).
- [102] C. Andreopoulos, C. Barry, S. Dytman, H. Gallagher, T. Golan, R. Hatcher, G. Perdue, and J. Yarba, The GENIE neutrino Monte Carlo generator: Physics and user manual, [arXiv:1510.05494](#).
- [103] P. S. B. Dev, D. Kim, K. Sinha, and Y. Zhang, New interference effects from light gauge bosons in neutrino-electron scattering, *Phys. Rev. D* **104**, 075001 (2021).
- [104] A. Ismail, R. Mammen Abraham, and F. Kling, Neutral current neutrino interactions at FASER ν , *Phys. Rev. D* **103**, 056014 (2021).
- [105] W. Bai, M. Diwan, M. V. Garzelli, Y. S. Jeong, and M. H. Reno, Far-forward neutrinos at the Large Hadron Collider, *J. High Energy Phys.* **06** (2020) 032.
- [106] T. Pierog, I. Karpenko, J. M. Katzy, E. Yatsenko, and K. Werner, EPOS LHC: Test of collective hadronization with data measured at the CERN Large Hadron Collider, *Phys. Rev. C* **92**, 034906 (2015).
- [107] K. Jodłowski, F. Kling, L. Roszkowski, and S. Trojanowski, Extending the reach of FASER, MATHUSLA, and SHiP towards smaller lifetimes using secondary particle production, *Phys. Rev. D* **101**, 095020 (2020).
- [108] V. Shtabovenko, R. Mertig, and F. Orellana, FeynCalc 9.3: New features and improvements, *Comput. Phys. Commun.* **256**, 107478 (2020).
- [109] A. Buckley, J. Ferrando, S. Lloyd, K. Nordström, B. Page, M. Rüfenacht, M. Schönherr, and G. Watt, LHAPDF6: Parton density access in the LHC precision era, *Eur. Phys. J. C* **75**, 132 (2015).
- [110] E. Rodrigues, The Scikit-HEP project, *EPJ Web Conf.* **214**, 06005 (2019).